Kamleh, Waseem Rolf; Bowman, Patrick Oswald; Leinweber, Derek Bruce; Williams, Anthony Gordon; Zhang, Jianbo
Unquenching effects in the quark and gluon propagator Physical Review D, 2007; 76(9):094501

http://link.aps.org/doi/10.1103/PhysRevD.76.094501

Unquenching effects in the quark and gluon propagator

Waseem Kamleh,[1,2] Patrick O. Bowman,[3] Derek B. Leinweber,[1] Anthony G. Williams,[1] and Jianbo Zhang[1,4]

[1]*Special Research Centre for the Subatomic Structure of Matter and Department of Physics, University of Adelaide 5005, Australia*

[2]*School of Mathematics, Trinity College, Dublin 2, Ireland*

[3]*Centre of Theoretical Chemistry and Physics, Institute of Fundamental Sciences, Massey University (Auckland), Private Bag 102904, NSMSC, Auckland, New Zealand*

[4]*ZIMP and Department of Physics, Zhejiang University, Hangzhou 310027, China*

(Received 25 May 2007; published 1 November 2007)

In this work we examine the fat-link irrelevant clover (FLIC) overlap quark propagator and the gluon propagator on both dynamical and quenched lattices. The tadpole-improved Luscher-Weisz gauge action is used in both cases. The dynamical gauge fields use the FLIC fermion action for the sea quark contribution. We observe that the presence of sea quarks causes a suppression of the mass function, quark renormalization function, and gluon dressing function in the infrared. The ultraviolet physics is unaffected.

DOI: 10.1103/PhysRevD.76.094501 PACS numbers: 12.38.Gc, 11.15.Ha, 12.38.Aw, 14.65.−q

Quark and gluon propagators are fundamental quantities in QCD encoding the rich nonperturbative and perturbative properties of QCD. In previous studies, the fat-link irrelevant clover (FLIC) overlap quark propagator and the gluon propagator were examined on quenched lattices [1–3]. In this work we study the effects of two flavor dynamical FLIC fermions [4] on these quantities for the first time.

The use of smeared or ''fat'' links in lattice fermion actions has been of interest for some time [5] and FLIC fermions [6,7] have shown a number of promising advantages over standard lattice actions. The FLIC fermion action is a Wilson-clover type fermion action in which the irrelevant operators of the Wilson and clover terms are constructed using fat links, while the relevant operators use the untouched (thin) gauge links. By smearing only the irrelevant, higher dimensional terms in the action, and leaving the relevant dimension-four operators untouched, short distance quark and gluon interactions are retained.

Fat links may be created by any number of smearing prescriptions including APE smearing [8–11], hypercubic smearing [12], stout-link smearing [13], or the unit-circle smearing [4] used herein.

The use of fat links in the FLIC action minimizes the effect of renormalization on the action improvement terms. Scaling studies indicate FLIC fermions provide a new form of nonperturbative $\mathcal{O}(a)$ improvement [14] where near-continuum results are obtained at finite lattice spacing.

Access to the light quark mass regime is enabled by the improved chiral properties of the lattice fermion action [15]. In particular, the histogram of the additive mass renormalization encountered in chiral-symmetry breaking Wilson-type fermion actions is seen to narrow upon introducing fat links in the irrelevant operators. These benefits facilitate the generation of the dynamical fermion configurations examined herein.

I. CONTINUUM PROPAGATORS

We begin by reviewing the formulation of the quark and gluon propagator on the lattice. In the continuum, the tree-level ($A_\mu(x) = 0$) quark propagator is identified with the (Euclidean space) fermionic Greens function,

$$(\not{\partial} + m^0)\Delta_{\mathrm{f}}(x, y) = \delta^4(x - y), \tag{1}$$

where m^0 is the bare quark mass. In momentum space this equation is solved straightforwardly,

$$\tilde{\Delta}_{\mathrm{f}}(p) = \frac{1}{i\not{p} + m^0}. \tag{2}$$

Denote $S^{(0)}(p) \equiv \tilde{\Delta}_{\mathrm{f}}(p)$ to be the tree-level propagator in momentum space. Then in the presence of gauge field interactions, define $S_{\mathrm{bare}}(p)$ to be the Fourier transform of the (interacting) fermionic Green's function,

$$(\not{\partial} + m^0)\Delta_{\mathrm{f}}^{\mathrm{bare}}(x, y) = \delta^4(x - y). \tag{3}$$

We define the mass function $M(p)$ and the bare renormalization function $Z(p)$ such that the bare quark propagator has the form

$$S_{\mathrm{bare}}(p) = \frac{Z(p)}{i\not{p} + M(p)}. \tag{4}$$

Then for the renormalization point ζ, the renormalized quark propagator is given by

$$S_\zeta(p) = \frac{Z_\zeta(p)}{i\not{p} + M(p)} = Z_2(\zeta, a)S_{\mathrm{bare}}(p), \tag{5}$$

where $Z_\zeta(p)$ is the (ζ-dependent) renormalization function, and $Z_2(\zeta, a)$ is the wave function renormalization constant, which depends on ζ and the regulator parameter a. The a-dependence of S_{bare} is implicit. $Z_2(\zeta, a)$ is chosen such that

$$Z_\zeta(p)|_{p^2=\zeta^2} = 1. \quad (6)$$

As $S_\zeta(p)$ is multiplicatively renormalizable, all of the ζ-dependence is contained within $Z_\zeta(p)$, that is, the mass function is ζ-independent.

The continuum tree-level gluon propagator in Landau gauge is associated with the following Greens function,

$$(\delta^{\mu\nu}\partial^2 - \partial^\mu\partial^\nu)\delta_{ab}D^{(0)ab}{}_{\mu\nu}(x, y) = \delta^4(x - y). \quad (7)$$

In momentum space the tree-level gluon propagator takes the form,

$$D^{(0)ab}{}_{\mu\nu}(q) = \left(\delta_{\mu\nu} - \frac{q_\mu q_\nu}{q^2}\right)\delta^{ab}\frac{1}{q^2}. \quad (8)$$

The nonperturbative gluon propagator is defined as the following two-point function,

$$D^{ab}_{\mu\nu}(x, y) = \langle A^a_\mu(x)A^b_\nu(y)\rangle. \quad (9)$$

The scalar propagator $D(q^2)$ is related to the full propagator (in momentum space) by

$$D^{ab}_{\mu\nu}(q) = \left(\delta_{\mu\nu} - \frac{q_\mu q_\nu}{q^2}\right)\delta^{ab}D(q^2). \quad (10)$$

The renormalized scalar propagator $D_\xi(q^2)$ is chosen such that at some momentum scale ξ,

$$q^2D_\xi(q^2)|_{q^2=\xi^2} = 1. \quad (11)$$

We refer to $q^2D_\xi(q^2)$ as the gluon dressing function.

II. FLIC OVERLAP FERMIONS

The overlap formalism [16–19] in the vectorlike case leads to the following definition of the massless overlap-Dirac operator [20],

$$D_o = \frac{1}{2a}(1 + \gamma_5\epsilon(H)). \quad (12)$$

Here, $\epsilon(H)$ is the matrix sign function applied to the overlap kernel H. The kernel can be any Hermitian version of the Dirac operator which represents a single fermion species of large negative mass. The standard choice is the Hermitian Wilson-Dirac operator (setting $a = 1$),

$$H_w = \gamma_5(\nabla\!\!\!/ + \tfrac{1}{2}\Delta - m_w), \quad (13)$$

where $\nabla\!\!\!/$ is the central covariant finite difference operator, and Δ is the lattice Laplacian, or Wilson term. The lattice gauge covariant derivative is defined by

$$\nabla\!\!\!/ = \sum_\mu \frac{1}{2}\gamma_\mu(U_\mu(x)\delta_{x+\hat\mu,y} - U^\dagger_\mu(x - \hat\mu)\delta_{x-\hat\mu,y}), \quad (14)$$

and likewise the lattice Laplacian is such that

$$\Delta = \sum_\mu 2 - (U_\mu(x)\delta_{x+\hat\mu,y} + U^\dagger_\mu(x - \hat\mu)\delta_{x-\hat\mu,y}). \quad (15)$$

In this work, as in previous studies, we use the FLIC action [6,7] as the overlap kernel [1]. The FLIC fermion action is a variant of the clover action where the irrelevant operators are constructed using APE-smeared links [8–11], and mean field improvement [21] is performed. The Hermitian FLIC operator is given by

$$H_{flic} = \gamma_5(\nabla\!\!\!/_{mfi} + \tfrac{1}{2}(\Delta^{fl}_{mfi} - \tfrac{1}{2}\sigma\cdot F^{fl}_{mfi}) - m_w), \quad (16)$$

where the presence of fat (smeared) links and/or mean field improvement has been indicated by the super- and subscripts. We choose $\sigma_{\mu\nu} = \frac{i}{2}[\gamma_\mu, \gamma_\nu]$ and use a standard one-loop $F_{\mu\nu}$,

$$F_{\mu\nu}(x) = -\frac{i}{2}(C_{\mu\nu}(x) - C^\dagger_{\mu\nu}(x)), \quad (17)$$

$$C_{\mu\nu}(x) = \tfrac{1}{4}(U_{\mu,\nu}(x) + U_{-\nu,\mu}(x) + U_{\nu,-\mu}(x) + U_{-\mu,-\nu}(x)), \quad (18)$$

where $U_{\mu,\nu}(x)$ is the elementary plaquette in the $+\mu$, $+\nu$ direction.

The APE-smeared links $U^{fl}_\mu(x)$ constructed from $U_\mu(x)$ by performing n smearing sweeps, where in each sweep we first perform an APE blocking step,

$V^{(j)}_\mu(x) = (1-\alpha)$ $+ \frac{\alpha}{6}\sum_{\nu\neq\mu}$ $+$  ,

followed by a projection back into $SU(3)$, $U^{(j)}_\mu(x) = \mathcal{P}(V^{(j)}_\mu(x))$. In this work, the projection is defined by first performing a projection into $U(3)$,

$$U'(V) = V[V^\dagger V]^{-(1/2)}, \quad (20)$$

and then projection into $SU(3)$,

$$\mathcal{P}(V) = \frac{1}{\sqrt[3]{\det U'(V)}}U'(V). \quad (21)$$

As it is only the product $n\alpha$ that matters [22], we fix $\alpha = 0.7$ and only vary n.

Mean field improvement is performed by making the replacements

$$U_\mu(x) \to \frac{U_\mu(x)}{u_0}, \qquad U^{fl}_\mu(x) \to \frac{U^{fl}_\mu(x)}{u^{fl}_0}, \quad (22)$$

where u_0 and u^{fl}_0 are the mean links for the standard and smeared gauge fields. We calculate the mean link via the fourth root of the average plaquette,

$$u_0 = \langle\tfrac{1}{3}\mathrm{Re\,Tr}U_{\mu\nu}(x)\rangle^{1/4}_{x,\mu<\nu}. \quad (23)$$

III. LATTICE QUARK PROPAGATOR

It is easily seen that the continuum massless quark propagator anticommutes with γ_5,

$$\{\gamma_5, S^{c}_{\text{bare}}(p)|_{m^0=0}\} = 0. \tag{24}$$

A straightforward consequence of the Ginsparg-Wilson relation is the inverse of the overlap Dirac operator satisfies

$$\{\gamma_5, D_o^{-1}\} = 2\gamma_5. \tag{25}$$

Noting that the mean link is a function of a and that $u_0(a)$, $u_0^{\text{fl}}(a) \to 1$ as $a \to 0$, we obtain

$$\lim_{a\to 0} D_o = \frac{1}{2m_w} \not{p}. \tag{26}$$

It is then natural to define the (external) massless bare overlap propagator on the lattice as [19,23]

$$S_{\text{bare}}(p)|_{m^0=0} \equiv \frac{1}{2m_w}(D_o^{-1} - 1), \tag{27}$$

as we then have that

$$\{\gamma_5, S_{\text{bare}}(p)|_{m^0=0}\} = 0, \tag{28}$$

as in the continuum case. The massive overlap Dirac operator is given by [24]

$$D_o(\mu) = (1 - \mu)D_o + \mu, \tag{29}$$

with $|\mu| < 1$ representing fermions of mass $\propto \frac{\mu}{1-\mu}$. The massive (external) bare overlap propagator is defined as [23]

$$S_{\text{bare}}(p) \equiv \frac{1}{2m_w(1-\mu)}(D_o^{-1}(\mu) - 1), \tag{30}$$

and with the identification

$$\mu = \frac{m^0}{2m_w} \tag{31}$$

satisfies

$$S^{-1}_{\text{bare}}(p) = S^{-1}_{\text{bare}}(p)|_{m^0=0} + m^0. \tag{32}$$

In order to construct $M(p)$ and $Z(p)$ on the lattice, we first define $\mathcal{B}(p)$, $\mathcal{C}_\mu(p)$ such that

$$S_{\text{bare}}(p) = -i\not{\mathcal{C}}(p) + \mathcal{B}(p). \tag{33}$$

Then

$$\mathcal{C}_\mu(p) = \frac{i}{n_s n_c}\,\text{Tr}[\gamma_\mu S_{\text{bare}}(p)], \tag{34}$$

$$\mathcal{B}(p) = \frac{1}{n_s n_c}\,\text{Tr}[S^{\text{bare}}(p)], \tag{35}$$

where the trace is over color and spinor indices only, and n_s, n_c specify the dimension of the spinor and color vector spaces. Now, define the functions $B(p)$, $C_\mu(p)$ such that the inverse of the bare (lattice) quark propagator has the form

$$S^{-1}_{\text{bare}}(p) = i\not{C}(p) + B(p). \tag{36}$$

Then it is easily seen that

$$C_\mu = \frac{\mathcal{C}_\mu}{\mathcal{C}^2 + \mathcal{B}^2}, \qquad B = \frac{\mathcal{B}}{\mathcal{C}^2 + \mathcal{B}^2}, \tag{37}$$

where $\mathcal{C}^2 = \mathcal{C}\cdot\mathcal{C}$.

The kinematical lattice momentum q_μ is defined such that at tree-level

$$(S^{(0)})^{-1}(p) = i\not{q} + m^0, \tag{38}$$

that is $q_\mu(p) = C^{(0)}_\mu(p)$, $m^0 = B^{(0)}(p)$. We note that the simple form of these relations is one of the advantages of overlap fermions, as the absence of additive mass renormalization prevents the need for having to perform any tree-level correction [25] (necessary most other fermions actions [26–28]), outside of identifying the correct momentum variable q. Now, we define $A(p)$ such that

$$S^{-1}_{\text{bare}}(p) = i\not{q}A(p) + B(p). \tag{39}$$

The mass function $M(p)$ and renormalization function $Z(p)$ may then be straightforwardly constructed,

$$Z(p) = \frac{1}{A(p)}, \qquad M(p) = \frac{B(p)}{A(p)}. \tag{40}$$

IV. LATTICE GLUON PROPAGATOR

We use a tadpole-improved plaquette plus rectangle gluon action,

$$S^{\text{imp}}_{\text{gauge}} = \frac{5}{9}\beta \sum_{x\in L}\sum_{\mu<\nu} \text{Re}\,\text{Tr}\Big[(1 - U_{\mu\nu}(x)) - \frac{1}{20u_0^2}(2 - R^{(2\times1)}_{\mu\nu}(x) - R^{(1\times2)}_{\mu\nu}(x))\Big]. \tag{41}$$

The lattice gauge field may be related to a continuum gauge field through a path ordered exponential,

$$U_\mu(x) = \mathcal{P} e^{ig\int_x^{x+e_\mu} dx_\mu A_\mu(x)}. \tag{42}$$

We can recover the lattice gluon field through the following ''midpoint'' definition,

$$A_\mu\Big(x + \frac{1}{2}e_\mu\Big) = \frac{1}{2ig}(U_\mu(x) - U^\dagger_\mu(x)) - \frac{1}{6ig}\,\text{Tr}(U_\mu(x) - U^\dagger_\mu(x)) + \mathcal{O}(a^2). \tag{43}$$

As in the continuum, the lattice gluon propagator in coordinate space is then given by

$$D^{ab}_{\mu\nu}(x, y) = \langle A^a_\mu(x) A^b_\nu(y)\rangle. \tag{44}$$

A Fourier transform takes us to momentum space, and we calculate the scalar propagator $D(q^2)$ directly. Tree-level improvement of the scalar gluon propagator is performed by identifying the appropriate kinematical momenta q such that

$$D^{(0)}(q^2) = \frac{1}{q^2}. \quad (45)$$

We denote the two different (gluonic and fermionic) kinematical momentum by q, and use context to distinguish them.

V. SIMULATION DETAILS

Calculations are performed on two quenched and two dynamical lattices. The dynamical lattices use a FLIC fermion action for the two degenerate flavors of sea quark. All the lattices have approximately the same physical volume, and the details of all lattices are given in Table I. Two lattice volumes are used, $12^3 \times 24$ and $16^3 \times 32$, with the lattice spacings for the quenched and dynamical lattices approximately matched. Landau gauge is chosen for the gauge fixing. An improved gauge fixing scheme [29] is used, and a conjugate gradient Fourier acceleration [30] algorithm is chosen to perform the gauge fixing.

Each lattice ensemble consists of 50 configurations. The lattice fermionic Green's function is obtained by inverting the FLIC overlap Dirac operator on each configuration using a multi-mass CG inverter [31]. We use periodic boundary conditions in the spatial directions and antiperiodic in the time direction. The Fourier transform is taken to convert to momentum space, and the bare quark propagator is obtained from the ensemble average. The quark propagator is calculated for 15 different masses. The details of the FLIC overlap parameters used are presented in Table II. The matrix sign function in the FLIC overlap is evaluated using the Zolotarev rational polynomial approximation [32], of degree (typically 8) chosen to give an accuracy of 2.0×10^{-8} within the spectral range of the kernel, after projecting out low-lying modes. The tree-level propagator is calculated by setting the links and the mean link to unity (the free theory). The kinematical lattice momentum q is obtained numerically from the tree-level propagator, although it could equally well have been obtained from the analytic form for q derived in Ref. [25].

The gluon propagator is obtained by performing a Fourier transform of the lattice gluon field A_μ using the midpoint definition and then calculating the scalar propagator directly.

TABLE II. The 15 lattice mass parameters μ used for each a. Values are chosen so that the bare masses are approximately matched for each lattice.

μ	$a = 0.120$	$a = 0.096$
μ_1	0.004 00	0.003 05
μ_2	0.008 00	0.006 10
μ_3	0.012 00	0.009 15
μ_4	0.016 00	0.012 20
μ_5	0.020 00	0.015 25
μ_6	0.024 00	0.018 30
μ_7	0.028 00	0.021 34
μ_8	0.032 00	0.024 39
μ_9	0.040 00	0.030 49
μ_{10}	0.048 00	0.036 59
μ_{11}	0.060 00	0.045 74
μ_{12}	0.080 00	0.060 98
μ_{13}	0.100 00	0.076 23
μ_{14}	0.120 00	0.091 48
μ_{15}	0.140 00	0.106 72

VI. RESULTS

We first examine the gluon propagator results. Figure 1 shows the bare gluon dressing function $q^2 D(q^2)$ on each of the lattices. The squares represent momenta entirely in a spatial Cartesian direction while triangles indicate points where the momentum is entirely along the temporal axis. The separation between these is due to the use of an asymmetric lattice and is a clear indication of finite volume effects. This is to be expected on such small physical volumes. The quenched and dynamical renormalized gluon dressing functions $q^2 D_\xi(q^2)$ are compared directly in Fig. 2. We see that the presence of dynamical quarks causes the suppression of the dressing function in the infrared. This effect is clear even with the relatively heavy sea quarks used in this study. The same effect was seen in work which compared the gluon propagator on quenched and dynamical lattices with a staggered fermion action [33,34].

We now turn to the quark propagator results. The mass function $M(p)$ and the renormalization function $Z_\zeta(p)$ are calculated on each of the lattices. As in previous studies, we apply a cylinder cut [25] to all the data, to reduce the

TABLE I. Parameters for the different lattices. All use a tadpole-improved Luscher-Weisz gluon action. Lattice spacings are set via a string tension analysis incorporating the lattice Coulomb term. Shown is the lattice volume, gauge coupling β, lattice spacing, pion mass (for the dynaical quarks) in MeV, the mean link, and the physical volume.

Volume	β	κ_{sea}	a(fm)	m_π	u_0	Phys. Vol. (fm^4)
$12^3 \times 24$	4.60	0.0000	0.120	∞	0.8888	$1.44^3 \times 2.88$
$16^3 \times 32$	4.80	0.0000	0.096	∞	0.8966	$1.54^3 \times 3.08$
$12^3 \times 24$	4.00	0.1318	0.120	806	0.8338	$1.44^3 \times 2.88$
$16^3 \times 32$	4.20	0.1300	0.096	820	0.8745	$1.54^3 \times 3.08$

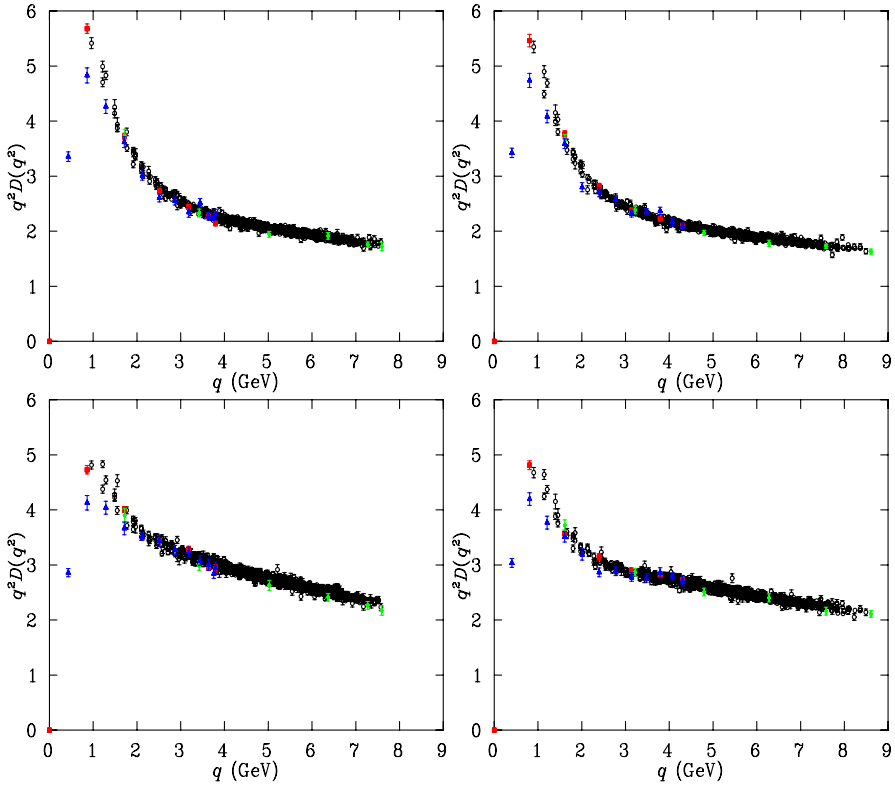

FIG. 1 (color online). Gluon propagator data for the bare gluon dressing function $q^2D(q^2)$. The quenched lattices are shown on the top and the dynamical lattices on the bottom. The left column shows the results for $a = 0.120$ and the right column for $a = 0.096$.

effects of rotational symmetry violation. An alternative method for reducing hypercubic artifacts is presented in [35]. The full results for the dynamical lattices are displayed in Fig. 3 for $M(p)$ and Fig. 5 for $Z_\zeta(p)$. The renormalization point ζ for $Z_\zeta(p)$ is chosen to be approximately $q = 6$ GeV. The full results for the quenched FLIC overlap quark propagator presented in previous work [1].

In order to compare the quenched and dynamical results, for each fixed momenta value we perform a quartic fit of both $M(p)$ and $Z(p)$ as a function of the pion mass (excluding the lightest two masses for finite volume reasons). The data and fits for the smallest 10 momenta on each of the lattices are shown in Fig. 4 for $M(p)$ and Fig. 6 for $Z(p)$. Having obtained the fit functions $M(p, m_\pi^2)$ and $Z(p, m_\pi^2)$ we then choose $m_\pi^2 = 0.0, 0.25, 0.5, 1.0, 2.0, 3.0$ GeV^2 and compare the functions at these values of the pion mass. In this way we can compare the quenched and dynamical results with matched pion masses. Results are shown in Figs. 7 and 8, to which we now turn our attention.

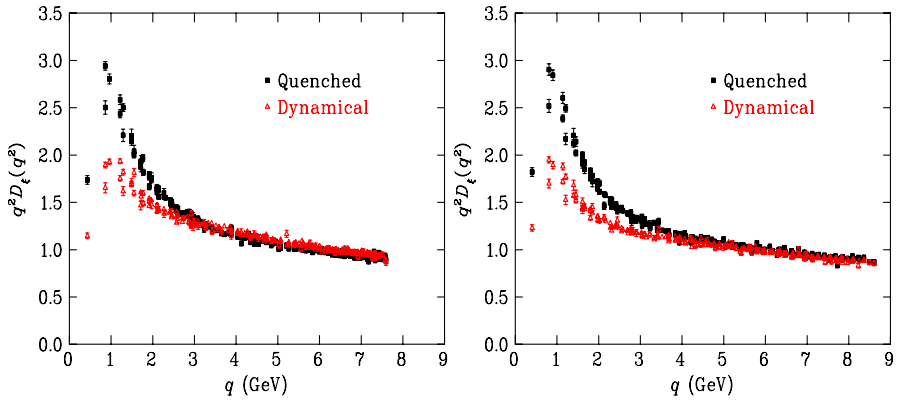

FIG. 2 (color online). Plots comparing the quenched (squares) and dynamical (triangles) renormalized gluon dressing function, $q^2D_\xi(q^2)$, for $a = 0.120$ (left) and $a = 0.096$ (right). The renormalization point ξ was chosen to be 6.0 GeV.

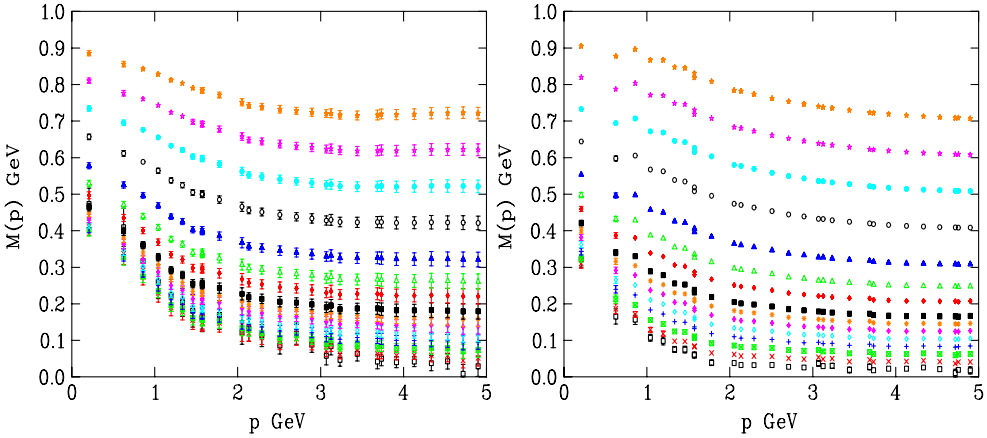

FIG. 3 (color online). Cylinder cut data for the dynamical FLIC Overlap mass function $M(p)$ at finite quark mass for the for the lattices at $a = 0.120$ (left) and $a = 0.096$ (right). The plots are against the discrete lattice momentum p.

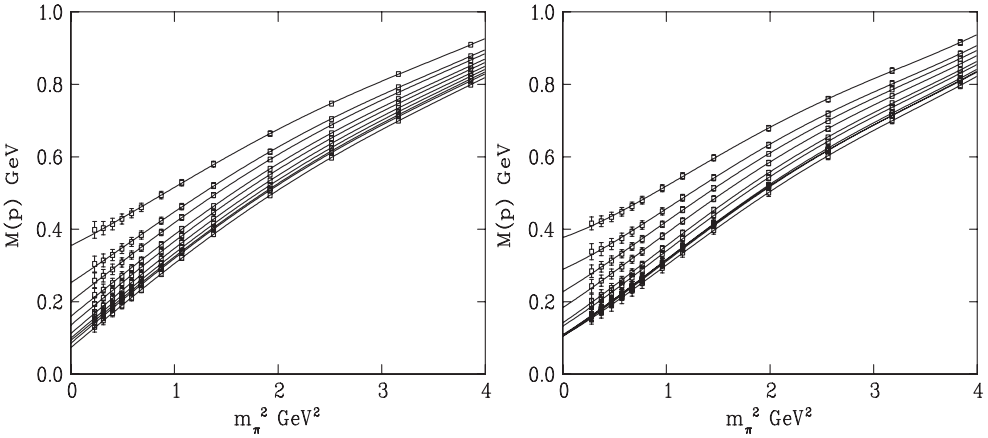

FIG. 4. Cylinder cut data showing the dependence of the mass function $M(p)$ for the quenched (left) and dynamical (right) FLIC overlap on the bare mass m^0 at fixed momenta, for the lowest 10 momenta values. At small bare mass, the curves are ordered inversely to the momenta they represent, that is the smallest momenta is the topmost curve. Data is shown for the lattices at $a = 0.120$ (top) and $a = 0.096$ (bottom). The solid curves are the quartic fits to the data.

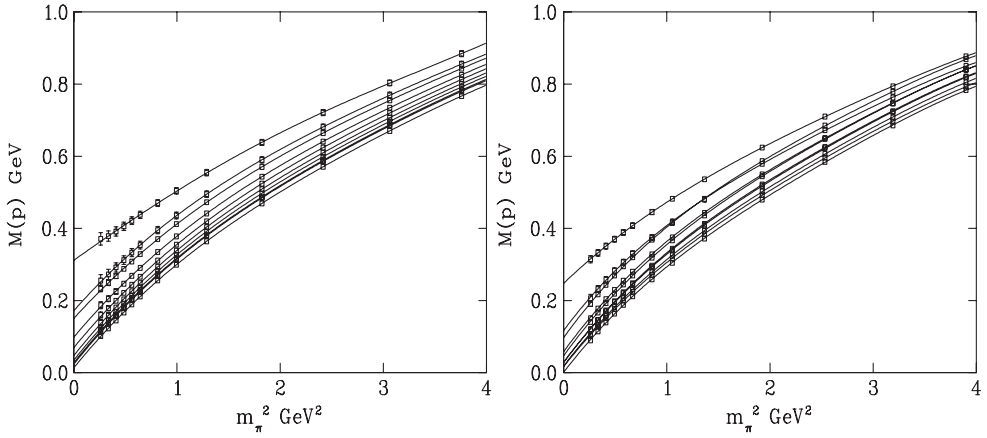

FIG. 5. Cylinder cut data for the dynamical renormalization function $Z_\zeta(q)(\zeta = 6\text{GeV})$ at finite quark mass for the lattices at $a = 0.120$ (left) and $a = 0.096$ (right). The plots are against the kinematical lattice momentum q.

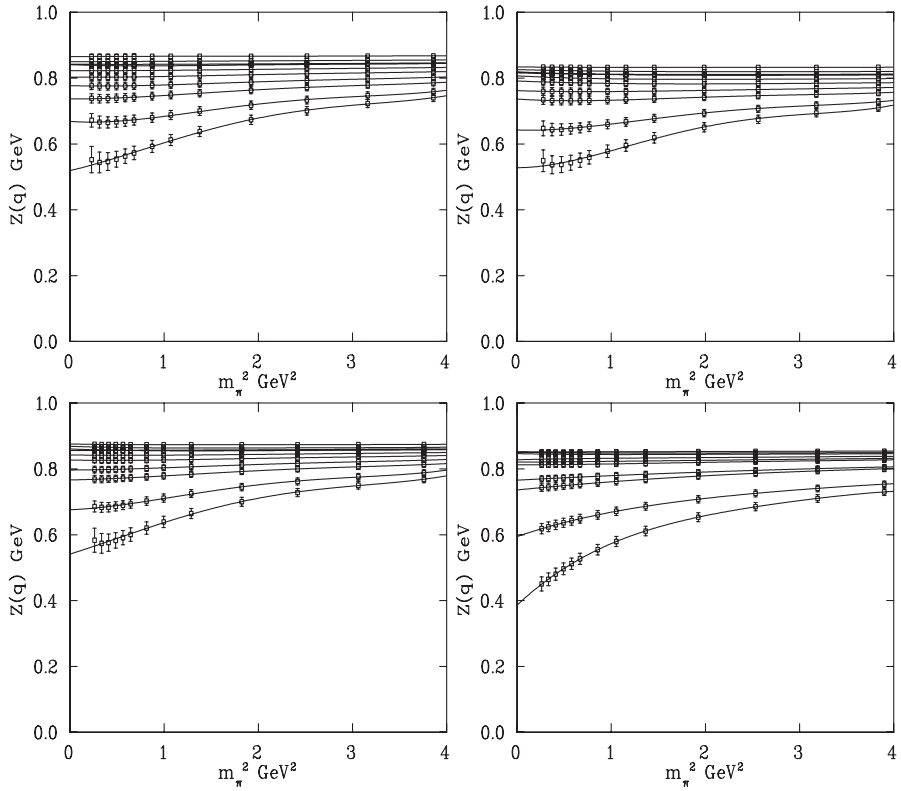

FIG. 6. Cylinder cut data showing the dependence of the renormalization function $Z(p)$ for the quenched (left) and dynamical (right) FLIC overlap on the pion mass m_π^2 at fixed momenta, for the lowest 10 momenta values. The curves are ordered according to the momenta they represent, that is the largest momenta is the topmost curve. Data is shown for the lattices at $a = 0.120$ (top) and $a = 0.096$ (bottom). The solid curves are the quartic fits to the data.

First we examine the mass function in Fig. 7. The results for $a = 0.120$ show little effect due to the presence of sea quarks, just a slight suppression in the infrared for the lighter masses. The heavier masses show essentially no difference between the quenched and dynamical results, except in the extreme ultraviolet, where the discretization errors give some difference. The discretization errors are not present in the $a = 0.096$ results, but now we can clearly see infrared suppression of $M(p)$ in the dynamical results for all masses.

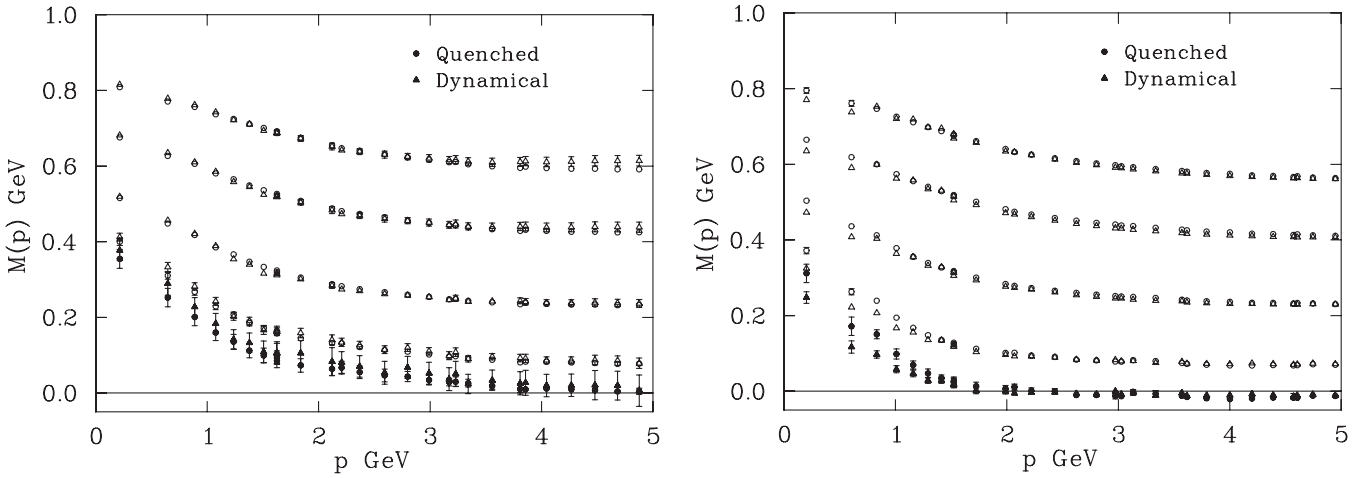

FIG. 7. Cylinder cut data comparing the interpolated mass function $M(p)$ for the dynamical and quenched lattices at $a = 0.120$ (left), $a = 0.096$ (right). The different curves from lowest to highest represent matched pion masses of $m_\pi^2 = 0.0, 0.3, 1.0, 2.0, 3.0$ GeV^2. The solid points indicate the chiral limit.

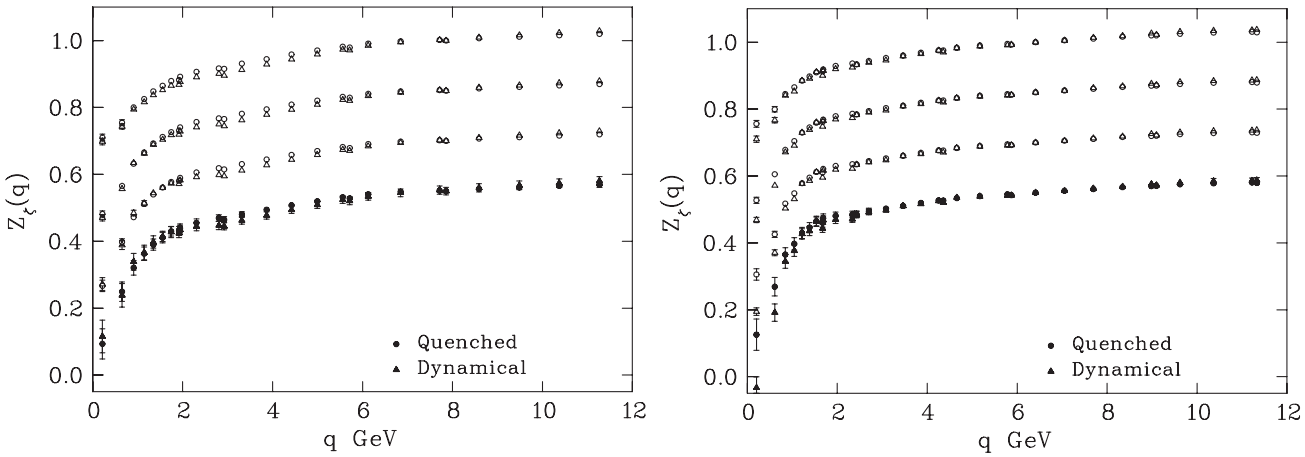

FIG. 8. Cylinder cut data comparing the interpolated renormalization function $Z_\zeta(q)$ for the dynamical and quenched lattices at $a = 0.120$ (left), $a = 0.096$ (right). The different curves from lowest to highest represent matched pion masses of $m_\pi^2 = 0.0, 0.3, 1.0, 2.0\ \mathrm{GeV}^2$. The solid points indicate the chiral limit. The different $Z_\zeta(q)$ have been offset vertically for clarity. The renormalization point is chosen to be $\zeta \approx 6$ GeV.

Turning to the renormalization function, Fig. 8 both the lattices show infrared suppression of $Z_\zeta(q)$ in the presence of dynamical quarks, and agreement in the far ultraviolet. At $a = 0.096$ the quenched and dynamical results also agree in the intermediate momentum regime, whereas there is a slight discrepancy in this region at $a = 0.120$.

VII. CONCLUSIONS

The gluon propagator and FLIC overlap quark propagator are compared on quenched and dynamical FLIC lattices at $a = 0.096$ and $a = 0.120$. We observe the presence of dynamical quarks causes suppression in the infrared in all quantities examined: the gluon dressing function $q^2D(q^2)$, the mass function $M(p)$ and the quark renormalization function $Z(q)$. Some differences between the results for the two lattice spacings indicate we are not quite in the scaling region at the coarser spacing. An alternative source of systematic error in the quark propagator results is the simplistic fitting functions used, which do not take into account the possibility of nonanalytic behavior at light quark mass. However, our results are consistent with those obtained elsewhere [33,34,36].

ACKNOWLEDGMENTS

We thank both the South Australian Partnership for Advanced Computing (SAPAC) and the Australian Partnership for Advanced Computing (APAC) for generous grants of supercomputer time which have enabled this project. This work is supported by the Australian Research Council. W. K. is supported by SFI basic research grant 04/BR/P0266. J. B. Z. is partly supported by Chinese NSFC-Grant No. 10675101.

[1] W. Kamleh, D. H. Adams, D. B. Leinweber, and A. G. Williams, Phys. Rev. D **66**, 014501 (2002).
[2] F. D. R. Bonnet, P. O. Bowman, D. B. Leinweber, A. G. Williams, and J. M. Zanotti, Phys. Rev. D **64**, 034501 (2001).
[3] F. D. R. Bonnet, P. O. Bowman, D. B. Leinweber, and A. G. Williams, Phys. Rev. D **62**, 051501 (2000).
[4] W. Kamleh, D. B. Leinweber, and A. G. Williams, Phys. Rev. D **70**, 014502 (2004).
[5] T. DeGrand, A. Hasenfratz, and T. G. Kovacs, Nucl. Phys. **B547**, 259 (1999).
[6] J. M. Zanotti *et al.* (CSSM Lattice), Phys. Rev. D **65**, 074507 (2002).
[7] W. Kamleh, Lect. Notes Phys. **663**, 65 (2005).
[8] M. Falcioni, M. L. Paciello, G. Parisi, and B. Taglienti, Nucl. Phys. **B251**, 624 (1985).
[9] M. Albanese *et al.* (APE), Phys. Lett. B **192**, 163 (1987).
[10] F. D. R. Bonnet, D. B. Leinweber, A. G. Williams, and J. M. Zanotti, Phys. Rev. D **65**, 114510 (2002).
[11] M. C. Chu, J. M. Grandy, S. Huang, and J. W. Negele, Phys. Rev. D **49**, 6039 (1994).
[12] A. Hasenfratz and F. Knechtli, Phys. Rev. D **64**, 034504 (2001).
[13] C. Morningstar and M. J. Peardon, Phys. Rev. D **69**, 054501 (2004).
[14] J. M. Zanotti, B. Lasscock, D. B. Leinweber, and A. G. Williams, Phys. Rev. D **71**, 034510 (2005).
[15] S. Boinepalli, W. Kamleh, D. B. Leinweber, A. G.

Williams, and J. M. Zanotti, Phys. Lett. B **616**, 196 (2005).
[16] R. Narayanan and H. Neuberger, Phys. Lett. B **302**, 62 (1993).
[17] R. Narayanan and H. Neuberger, Nucl. Phys. **B412**, 574 (1994).
[18] R. Narayanan and H. Neuberger, Phys. Rev. Lett. **71**, 3251 (1993).
[19] R. Narayanan and H. Neuberger, Nucl. Phys. **B443**, 305 (1995).
[20] H. Neuberger, Phys. Lett. B **417**, 141 (1998).
[21] G. P. Lepage and P. B. Mackenzie, Phys. Rev. D **48**, 2250 (1993).
[22] F. D. R. Bonnet, P. Fitzhenry, D. B. Leinweber, M. R. Stanford, and A. G. Williams, Phys. Rev. D **62**, 094509 (2000).
[23] R. G. Edwards, U. M. Heller, and R. Narayanan, Phys. Rev. D **59**, 094510 (1999).
[24] H. Neuberger, Phys. Rev. D **57**, 5417 (1998).
[25] F. D. R. Bonnet, P. O. Bowman, D. B. Leinweber, A. G. Williams, and J. B. Zhang (CSSM Lattice), Phys. Rev. D **65**, 114503 (2002).
[26] J. I. Skullerud and A. G. Williams, Phys. Rev. D **63**, 054508 (2001).
[27] J. Skullerud, D. B. Leinweber, and A. G. Williams, Phys. Rev. D **64**, 074508 (2001).
[28] P. O. Bowman, U. M. Heller, and A. G. Williams, Nucl. Phys. B, Proc. Suppl. **106**, 820 (2002).
[29] F. D. R. Bonnet, P. O. Bowman, D. B. Leinweber, A. G. Williams, and D. G. Richards, Aust. J. Phys. **52**, 939 (1999).
[30] A. Cucchieri and T. Mendes, Phys. Rev. D **57**, R3822 (1998).
[31] A. Frommer, B. Nockel, S. Gusken, T. Lippert, and K. Schilling, Int. J. Mod. Phys. C **6**, 627 (1995).
[32] T.-W. Chiu, T.-H. Hsieh, C.-H. Huang, and T.-R. Huang, Phys. Rev. D **66**, 114502 (2002).
[33] P. O. Bowman, U. M. Heller, D. B. Leinweber, M. B. Parappilly, and A. G. Williams, Phys. Rev. D **70**, 034509 (2004).
[34] P. O. Bowman *et al.*, Phys. Rev. D **71**, 054507 (2005).
[35] F. de Soto and C. Roiesnel, arXiv:0705.3523.
[36] C. S. Fischer and R. Alkofer, Phys. Rev. D **67**, 094020 (2003).